Marine Chemistry 228 (2021) 103906

Contents lists available at ScienceDirect

Marine Chemistry

journal homepage: www.elsevier.com/locate/marchem

Imaging of organic signals in individual fossil diatom frustules with nanoSIMS and Raman spectroscopy

Shaun P. Akse [a,*], Gobind Das [b,c], Susana Agustí [b], Laetitia Pichevin [d], Lubos Polerecky [a], Jack J. Middelburg [a]

[a] Department of Earth Sciences, Utrecht University, PO Box 80021, 3508 TA Utrecht, the Netherlands
[b] Red Sea Research Center and Core Labs, King Abdullah University for Science and Technology, Thuwal, Saudi Arabia
[c] Department of Physics, Khalifa University, Abu Dhabi, P.box-127788, United Arab Emirates
[d] University of Edinburgh, School of Geosciences, Grant Institute, James Hutton Road, Edinburgh EH9 3FE, United Kingdom

ARTICLE INFO

Keywords:
Biogenic silica
Diatom-bound organic matter
Marine sediments
NanoSIMS
Raman spectroscopy

ABSTRACT

The organic matter occluded in the silica of fossil diatom frustules is thought to be protected from diagenesis and used for paleoceanographic reconstructions. However, the location of the organic matter within the frustule has hitherto not been identified. Here, we combined high spatial resolution imaging by nanoSIMS and Raman microspectroscopy to identify where the organic material is retained in cleaned fossil diatom frustules. NanoSIMS imaging revealed that organic signals were present throughout the frustule but in higher concentrations at the pore walls. Raman measurements confirmed the heterogenous presence of organics but could not, because of lower spatial resolution, resolve the spatial patterns observed by nanoSIMS.

1. Introduction

Diatoms, a ubiquitous group of microalgae, construct frustules made of hydrated amorphous silica that can be preserved in the sediment record. The application of diatom frustule paleoproxies has increased greatly in the last decade. The nitrogen isotope composition of diatom frustules has been proposed as a proxy for nitrogen utilization and thus surface nutrient consumption (i.e., Horn et al., 2011a; Robinson et al., 2014). This proxy is based on the presence of different proteins (mainly pleuralins, silaffins and long-chain polyamines) necessary for silica sequestration that are incorporated into the diatom frustule during growth (Kröger et al., 2002; Hecky et al., 1973; Kröger and Poulsen, 2008; Bridoux and Ingalls, 2010). During a period of growth, phytoplankton draw down nutrient concentrations, resulting in an increase of residual nitrate $\delta^{15}N$ due to the fractionation of N isotopes during nutrient uptake (similar to Rayleigh distillation). The rise in $\delta^{15}N_{nitrate}$ with nutrient depletion is expected to be recorded in the biogenic silica (opal) produced by diatoms (De La Rocha, 2006). As such, high $\delta^{15}N_{diatom}$ indicates that a greater fraction of available nutrients (nitrate) has been consumed during the growing season (Shemesh et al., 1993).

It has been suggested that, in contrast to the bulk sediment, nitrogen encased within the diatom frustule is protected from diagenetic alteration and thus presents a more robust proxy (Shemesh et al., 1993; Sigman et al., 1999). These assumptions are based on observations such as similar relative amino acid abundances in the organic matter of fossil frustules and living diatoms (Shemesh et al., 1993), the apparent absence of diagenetic variability in frustule-bound N when compared to bulk sediment N content (Sigman et al., 1999), and high diatom-bound amino acid concentrations in silica-rich sediments relative to sediment traps (Ingalls et al., 2003). However, as of yet, it is unknown where exactly in the frustule this organic matter resides.

For $\delta^{15}N_{diatom}$ analysis, several precautions are generally taken to ensure that only the frustule-bound nitrogen is measured, including several harsh cleaning methods to remove any loose organic matter and diagenetic alteration (Hendry and Rickaby, 2008; Robinson et al., 2004). Despite this, questions remain regarding the nature of the occluded organic matter. The isotope composition of entombed organic matter may vary, for example, due to species-specific amino acid compositions (Des Combes et al., 2008) or species-specific fractionation (Horn et al., 2011b). Possible isotopic alteration of the occluded organic matter during diagenesis remains largely unexplored, but it has been shown that the diagenetic incorporation of metals does not affect the N isotope values of the frustule-bound organic matter (Ren et al., 2013).

* Corresponding author.
E-mail addresses: s.p.akse@uu.nl, shaun.akse@gmail.com (S.P. Akse), J.B.M.Middelburg@uu.nl (J.J. Middelburg).

https://doi.org/10.1016/j.marchem.2020.103906
Received 26 February 2020; Received in revised form 26 August 2020; Accepted 18 November 2020
Available online 11 December 2020

This study explores the use of high spatial resolution imaging techniques to identify where in the cleaned fossil diatom frustule the organic material is retained. Our approach involved the development and application of nanoSIMS imaging (nanoscale secondary ion mass spectrometry), thereafter additional validation was sought with Raman spectroscopy and Transmission Electron Microscopy (TEM). NanoSIMS allows imaging of elements with a lateral resolution down to 50 nm, but can be sensitive to 3D sample topography due to the design of the ion optics (Nuñez et al., 2018). Furthermore, NanoSIMS typically probes only the upper few nm of the sample due to the low primary ion beam currents used to achieve high lateral resolution. In contrast, the Raman technique integrates signals over larger depths in the sample, but has a distinctly poorer (μm scale) lateral resolution (Liang et al., 2016). However, by probing of chemical bonds, Raman spectroscopy allows identification of the molecular structure of samples. The TEM technique used for this study had a high lateral resolution (<1 nm) but did not have the sensitivity to image the presence of the organic signal. By combining the data from the nanoSIMS and Raman techniques, we image for the first time the presence of organic matter in thoroughly cleaned fossil frustules of centric diatoms and suggest patterns of its heterogenous distribution within the frustule.

2. Materials & methods

2.1. Materials

The samples for this study originate from sediment Core MD-022515. This core was retrieved from the Guaymas Basin (27°29.01 N; 112°04.46 W; 881 m water depth) during the MONA (Marges Ouest Nord Américaines) cruise of the R/*V* Marion Dufresne (International Marine Global Changes-IMAGES VIII) in June 2002 (Pichevin et al., 2012). The diatom frustules were collected from a core depth of 1161 cm, corresponding to an age of 12,450 years Before Present according to Pichevin et al. (2012). Cleaning of the samples was performed following published protocols (Hendry and Rickaby, 2008; Morley et al., 2004; Pichevin et al., 2014), and comprised both mechanical and chemical cleaning steps.

2.2. Sample preparation and selection

Purification of the diatom samples for analysis was performed following published cleaning methods (Ellwood and Hunter, 1999; Morley et al., 2004; Hendry and Rickaby, 2008). The procedure includes both mechanical and chemical cleaning steps. Approximately 0.5 to 1 g of sediment was subsampled into a 50 mL centrifuge tube. Carbonates and organic matter were removed at temperature of 75 °C using 5% HCl and 40% H_2O_2, respectively, prior to mechanical separation of the diatoms from clays and other terrigenous components. The mechanical step consists of elimination of large debris by sieving (at 10 and 75 μm), differential settling using a heavy liquid (density set at 2.1 g/mL) as well as screening of the sample under the microscope to check the purity of the obtained diatom fraction (Morley et al., 2004). The chemical cleaning includes 3 steps and is performed on the isolated diatom fraction to ensure the absence of terrigenous contamination on the diatom frustules. The reagents used for the cleaning process were 1% hydroxylamine chloride in acetic acid; 0.1% *w*/w NaF solution and 50% strong-acid solution of ultrapure HNO_3 and HCl as described in (Hendry and Rickaby, 2008). The absence of contamination was confirmed using an ion microprobe Cameca 4F at the university of Edinburgh (NERC facility).

To prepare the samples for nanoSIMS analysis, a needle-tip portion of the diatom frustules was pressed onto an ultra-clean indium foil (99.99% indium; Alfa Aesar; 0.05 mm thick) attached to an aluminium stub. The sample was subsequently coated with a 12 nm thick Au layer using a sputter coater (JOEL JFC-2300HR high resolution fine coater, JEOL FC-TM20 thickness controller). The sample was then imaged with a table-top SEM (JEOL JCM-6000PLUS NeoScope Benchtop SEM) operating at a 15-kV accelerating voltage to identify specimens suitable for further analysis (i.e., individual frustules with minimal 3D topography).

2.3. NanoSIMS imaging

Nanoscale secondary ion mass spectrometry was performed with the nanoSIMS 50L instrument (Cameca, France) operated at Utrecht University (see Nuñez et al. (2018) for a review of the method). Electron multiplier detectors were set using a standard (SPI Supplies, 02757-AB 59 Metals & Minerals Standard) to enable the detection of secondary ions $^{12}C^-$, $^{16}O^-$, $^{12}C^{14}N^-$, $^{28}Si^-$, $^{31}P^-$ and $^{32}S^-$ with the $^{133}Cs^+$ primary ion beam. Of these, $^{12}C^-$, $^{12}C^{14}N^-$, $^{31}P^-$ and $^{32}S^-$ were used to identify organics while $^{16}O^-$ and $^{28}Si^-$ were used to identify the silica of the frustule. Nitrogen was measured as a molecular ion CN^- because the atomic ion ^{14}N has a poor ionization efficiency. The secondary ion ratio images in this study use $^{16}O^-$ due to the stronger signal compared to $^{28}Si^-$.

Prior to the analysis of each target frustule, an area slightly larger than the region of interest was pre-sputtered with the primary ion beam (FCo current 20pA, ~360 s) to remove the gold coating and reach stable secondary ion yields. After pre-sputtering, the instrument was tuned with diaphragm and slit settings of D1-3, ES-3, AS-2, and EnS-1. The analysis was carried out in the imaging mode by rastering a high-energy $^{133}Cs^+$ ion beam (16 keV, 2pA FCo, nominal beamsize 50–150 nm; electron gun enabled) over a target area on the frustule (between 4 μm × 4 μm and 55 μm × 55 μm in size) and measuring the sputtered secondary ions at a resolution of either 128 × 128 or 256 × 256 pixels and with a dwell time of 1 ms/pixel. Target areas were measured multiple times (typically over 300–600 planes) to increase signals and provide depth resolution. Data processing and analysis were done with an updated version of the Look@nanoSIMS software (Polerecky et al., 2012).

During the initial method development stage, measurements targeted frustules of different species of centric and pennate diatoms. However, pennate diatom frustules proved difficult to measure with the NanoSIMS due to their pronounced 3D topography. Therefore, only data obtained from the fossil frustules of various centric diatom species are presented. The combination of the primary ion current, dwell time, and the number of measured planes did not allow measurements through the entire thickness of the frustule. Therefore, the frustule interior and exterior were targeted by separate measurements.

2.4. Validation techniques

Raman measurements were performed with the Horiba LabRam spectrometer at the King Abdullah University for Science and Technology. The sample was excited with a 473 nm laser line in the back-scattering configuration through a 100× objective allowing a lateral resolution of ~1 μm. Using a grating with 1800 grooves/mm, Raman spectra were collected in the range of 150–3300 cm^{-1} with a spectral resolution of 1.2 cm^{-1}. Initially, the interior of an individual frustule was analyzed in three spots to identify the primary signals present. This was followed by imaging analysis of the interiors and exteriors of several frustules with the step size varying between 0.5 and 2 μm and the size of the imaged areas varying between 8 μm × 8 μm and 15 μm × 15 μm. During imaging with the lower step size (0.5 μm and 1 μm) only the lower frequency range (up to 1700 cm^{-1}) was recorded, whereas the larger step size imaging also covered higher frequencies (around 3000 cm^{-1}) to include a prominent organic peak between 2826 and 3021 cm^{-1}. Data analyses were performed using the manufacturer's software LabSpec (version 6).

To further constrain the distribution of organics within the frustules we explored two ultrahigh resolution imaging techniques. First, we used an ultrahigh resolution (<1 nm) TEM to image the presence of organics at pore edges. For this, the FEI Titan 80–300 was used at the King

Abdullah University for Science and Technology, which was equipped for electron energy loss spectroscopy (EELS) and energy-dispersive X-ray spectroscopy (EDS), in order to determine the elemental composition of the sample. However, it was not possible to acquire sufficient signal and therefore the results are not presented in this manuscript. Second, a FEI Helios Nanolab G3 SEM at Utrecht University was used for ultrahigh resolution (~1 nm) imaging after focused ion beaming cutting of a centric diatom frustule.

3. Results

3.1. Identification of organics by Raman spectroscopy

The presence of organics in the silica matrix of a cleaned fossil diatom frustule was confirmed by Raman measurements in multiple spots on the frustule (Fig. 1; Table 1). Besides Raman peaks associated with tetrahedral Si—O—Si, Si—O—Si network, Si—OH stretching and aluminium, there was clear evidence for an organic component characterized by C—H deformation and valence vibrations at wavenumbers around 1425 and 2910 cm^{-1}. An indication for N═O stretching at ~1600 cm^{-1} was also present.

3.2. NanoSIMS imaging of frustules

After establishing the presence of organics with single point Raman analyses, the elemental distributions were imaged with nanoSIMS. Secondary ions CN^- (detected as $^{12}C^{14}N^-$) and O^- were used as a proxy for organics and silica, respectively. Generally, CN^- ions were detected throughout the frustule but showed significantly higher counts in ring-like structures around the pores and in hotspots scattered across the frustule or near the edges of the frustule (Fig. 2b and f). The patterns were similar for both the frustule interior and exterior, although the surface morphology differed markedly between the two sides (compare Fig. 2a–b and e–f). Similar patterns were also observed for other elements associated with organics including C and S (Fig. 2c–d and g–h). High-resolution SEM images revealed that, on the frustule interior, the ring-like structures were associated with a clear thickening of the silica matrix around the pore (see inset in Fig. 2a). The difference in contrast in the SEM images suggested that the silica matrix in these ring-like structures was different from the rest of the matrix, consistent with the ring-like patterns in the organic signals observed by NanoSIMS.

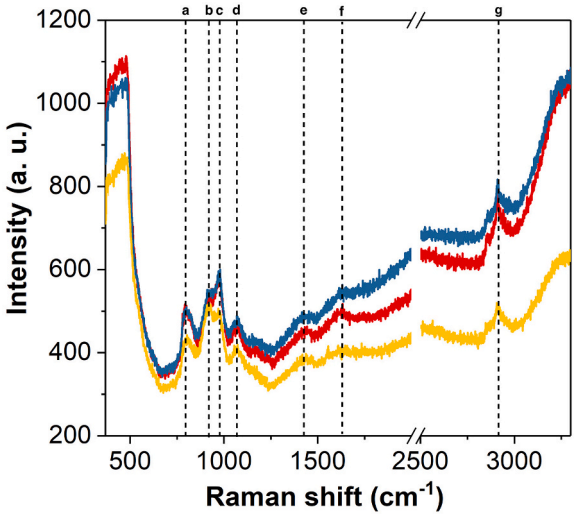

Fig. 1. Single point Raman spectra obtained from a cleaned fossil frustule of a centric diatom. Raman spectra were collected at three different locations on the silica of the interior frustule wall of a single specimen. Peak assignments are summarized in Table 1.

Table 1
Raman band assignments. Identification was based on (Terpstra et al., 1990; McMillan, 1982; Lin-Vien et al., 1991; Kammer et al., 2010; De Tommasi et al., 2018).

Band position (cm-1)	Band assignments
a) 768–848	Inter tetrahedral Si—O—Si
b) 870–952	Aluminium derivatives
c) 945–1010	Si—OH stretching
d) 1020–1134	Si—O—Si network
e) 1364–1438	δC-Hx
f) 1580–1640	N═O stretching
g) 2826–3021	νC-Hx

3.3. Mapping of organics by Raman spectroscopy

Although the signal around 2910 cm^{-1} had a stronger presence in the Raman spectra (Fig. 1), subsequent mapping focused on the peak at 1425 cm^{-1}, which allowed reduction in the frequency range and thus improved lateral resolution. Images obtained by Raman measurements showed pronounced heterogeneity in the signals corresponding to both the silica matrix and organics (Fig. 3). The intensity of the peaks corresponding to Si—OH and Si—O—Si appeared less variable than the intensity of the δC-Hx peak. Images of the peak ratio δC-Hx/Si—O—Si were heterogeneous (Fig. 3e), but even the lowest step size (0.5 μm step size) did not resolve the spatial patterns detected by NanoSIMS (compare Figs. 2 and 3). Raman images of the frustule interior and exterior appeared similar (Fig. 3).

4. Discussion

After performing the established mechanical and chemical cleaning steps, microscopic fossil diatom frustules were analyzed with different high-resolution imaging techniques to study the presence of remaining organics tightly bound to the silica matrix. For the first time, the presence of these organics was confirmed through imaging techniques. Furthermore, the chemical mapping capabilities of the techniques made it possible to resolve, to a variable degree, the patterns in the distribution of organics in the frustule. This revealed heterogeneity and it is suggested that this is due to enrichments around the pores.

4.1. NanoSIMS measurements

In this study, NanoSIMS proved to be the best option to map the spatial distribution of elements within the fragile frustules of diatoms. NanoSIMS images revealed intensification of organic signals at the pore edges of the (centric) diatom frustules (Fig. 2). The CN signal in particular, but also the signals of C and S, were clearly higher around the pores, and this spatial pattern remained as more material was sputtered away during the measurement (Supplementary Figs. S3 & S4). On the frustule interior, this signal enrichment is likely linked to the thickening of the silica matrix, which was often observed at the pore boundaries (Fig. 2a). As similar patterns were also observed on the frustule exterior, it is likely that the entire pore wall is marked by an increased organic presence (Fig. 4).

However, nanoSIMS measurements are known to be potentially sensitive to 3D topography of the sample surface, leading for instance to higher secondary count rates at or around the edges of the studied sample (e.g., Roepert, 2019; Nuñez et al., 2018). Thus, quantification should be avoided and a degree of caution is required when interpreting nanoSIMS data. Although we made a thorough and critical assessment of our data (Supplementary Figs. S3–S5)., including the analysis of lateral and depth variation in ion counts and ion count ratios, we cannot exclude that these "edge effects" played a role during the NanoSIMS measurements Other techniques without this caveat but with a comparable sensitivity and spatial resolution are needed to verify our results.

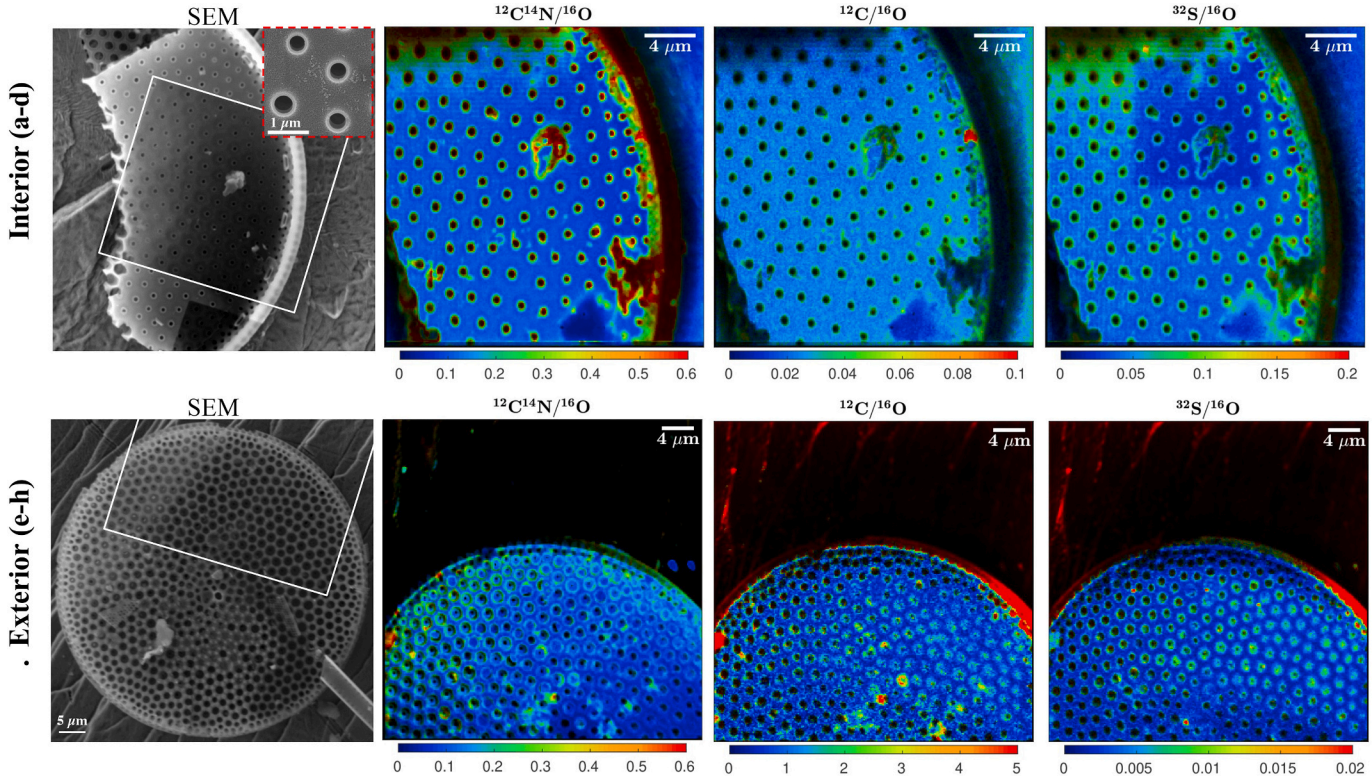

Fig. 2. NanoSIMS imaging of organic signals in cleaned fossil frustules of centric diatoms. Shown are SEM images of the frustule interior and exterior post NanoSIMS measurement, and the corresponding images of ion count ratios CN/O, C/O and S/O measured by NanoSIMS. White square in the SEM images indicates the area measured by NanoSIMS. Inset in panel a) shows a detailed SEM image of the pores using the FEI Helios Nanolab G3, measured on a different frustule than the one shown by the larger image (contrast slightly enhanced through image processing). Ion count images from which the ratio images were calculated are shown in Supplementary Fig. S1. Note that the intensity of the hue in the ratio images was modulated by the O ion count image to suppress noise from the background.

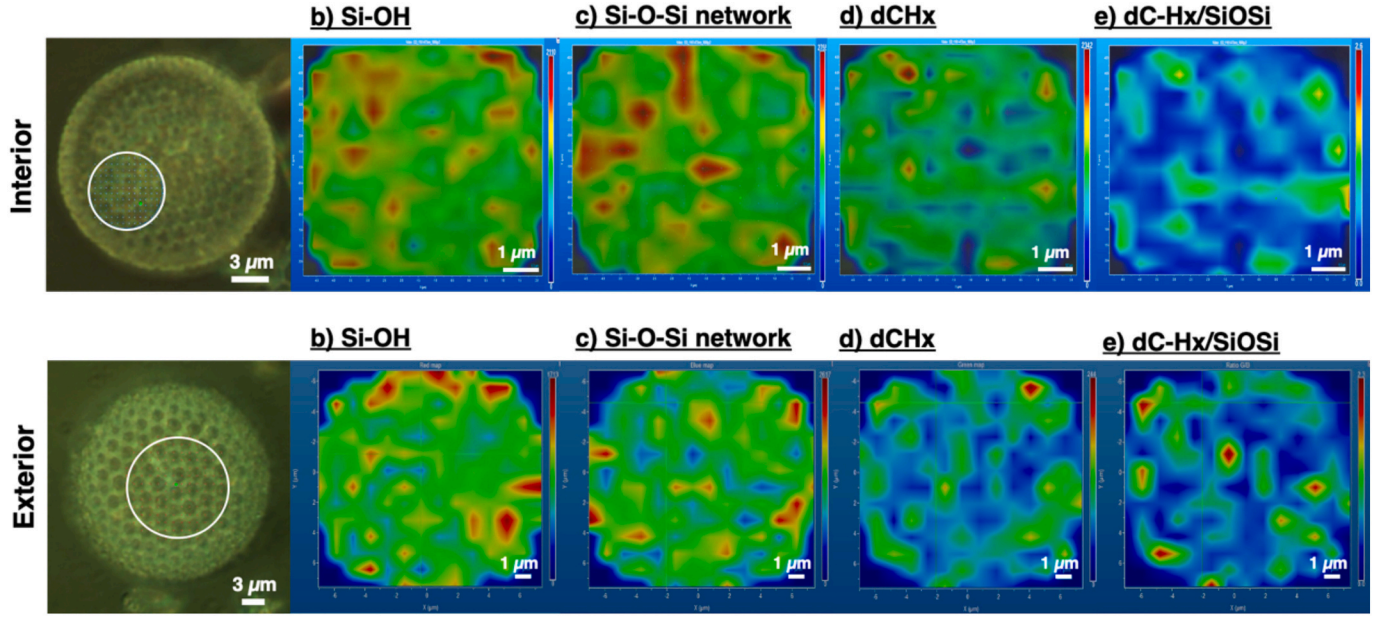

Fig. 3. Raman spectral mapping of cleaned fossil frustules of centric diatoms. Shown are maps of peak intensities corresponding to silica (Si—OH, Si—O—Si) and organics (δC-Hx), and the corresponding maps of the peak ratio δC-Hx/Si—O—Si. Maps from the frustule interior and exterior were acquired with the step-size of 0.5 μm and 1 μm, respectively. The measured areas (diameter of 8 μm and 15 μm) are marked in the corresponding optical image. Note that the images used an interpolation of values between the individual measured pixels. Lower resolution images are presented in Supplementary Fig. S2.

4.2. Validation

The nanoSIMS results presented in this study provide the first glimpse of the spatial distribution of organic matter bound to the silica matrix in fossil diatom frustules. In an attempt to validate these results, we looked towards additional high spatial resolution imaging

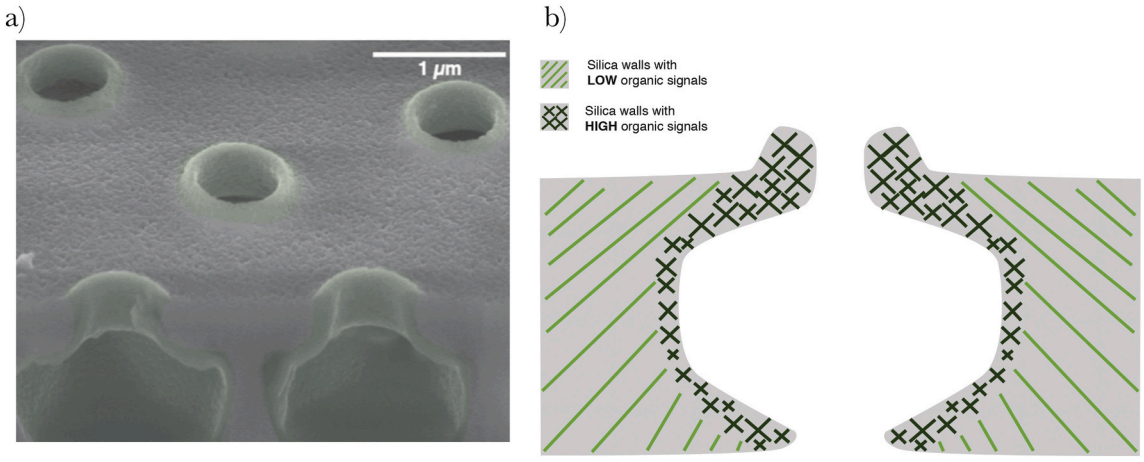

Fig. 4. Conceptual schematic illustrating the proposed distribution of organics in fossil frustules of centric diatoms. Shown is (a) an altered high-resolution SEM image of a centric diatom frustule, cut with a focused ion beam, and (b) a conceptual diagram of the pore cross-section. Organic signals are present throughout the silica (grey/striped) but higher concentrations are present at the pore walls (green/crosses). (For interpretation of the references to colour in this figure legend, the reader is referred to the web version of this article.)

techniques. As mentioned in Section 2.4 (Material and Methods), we have explored the use of the ultrahigh resolution FEI Titan 80–300 TEM to image the presence of organics at pore edges with an even greater spatial resolution (<1 nm). However, it was not possible to acquire sufficient signal for organics and thus the results are not presented in this manuscript. Focused-ion beam SEM imaging at high resolution confirmed differences in density between pore-edges and the remaining of the diatom frustule (Fig. 2A inset), consistent with nanoSIMS results.

Being aware of the limited spatial resolution, Raman spectroscopy was employed for resolving the concerns surrounding potential 3D-topography in nanoSIMS measurements. The Raman technique is also surface-specific, but it integrates the signal over a larger depth interval (~μm) and is thus less likely affected by potential edge effects. Raman measurements confirmed the presence of organic signals in cleaned fossil frustules, and indicated that they are heterogeneously distributed within the silica matrix. While the heterogeneity observed by nanoSIMS was confirmed, the lateral resolution of the Raman imaging (down to 0.5 μm) was insufficient to confirm or reject the spatial patterns observed around the pores.

While we applied several state-of-the-art techniques, there are additional techniques, or combinations of techniques, that could be explored in future research now that the presence of organics has been confirmed. There is clear value in combining, for example, scanning probe microscopy and Time-of-flight SIMS. Liang et al. (2016) gives an overview of the different techniques and how they can be used to simultaneously acquire morphological and chemical information. This may be a promising avenue to learn more about the nature of the observed organics around the pores.

4.3. Implications

An increased presence of organics at the pore walls (Fig. 4) may be due to a combination of the biomineralization process and the exchange of nutrients, through the pores, between the diatom cell and the surrounding water. During silicification, a protein template forms the basis onto which the silica frame is secreted (Hildebrand et al., 2018; Thamatrakoln and Hildebrand, 2008). An imaging study of the insoluble organic matrix (Tesson and Hildebrand, 2013) found that the pores of a diatom valve can be occluded by this material. Based on these observations, it is hypothesised that, during growth, the pores are not open channels but are instead lined or completely occluded by the organic material.

The samples investigated were thoroughly cleaned involving well-established multiple mechanical and chemical cleaning steps (Pichevin et al., 2014) that should have removed any superficial organic material remaining in fossil frustules. Furthermore, additional thorough pre-sputtering of the sample would aid in the removal of potential contaminants. Indeed, high-resolution imaging, in particular with nanoSIMS, clearly showed organics (in particular $^{12}C^{14}N$) that remained throughout the measurement (Supplementary Figs. S3 & S4) and are likely embedded in the silica matrix and concentrated around pore walls. This material is most likely the carrier for proxies such as $\delta^{15}N$.

5. Conclusions

This study explored the combination of high-resolution imaging techniques to document, for the first time, the presence and distribution of organic signals inside the silica matrix of individual fossil diatom frustules. NanoSIMS imaging suggested that organic signals were present throughout the frustule but in higher concentrations at the pore walls. Raman measurements confirmed the heterogeneous presence of organics but could not resolve the spatial patterns observed by nanoSIMS. This study shows that the organic material embedded in the silica matrix of fossil frustules can be imaged. The combination of nanoSIMS, Raman spectroscopy and other high-resolution imaging techniques may be used for future studies to improve our understanding of the $\delta^{15}N_{diatom}$ paleoproxy method. However, nanoSIMS analysis should be combined with additional high spatial resolution chemical mapping techniques to confirm and better understand the distribution of organics within the frustule of fossil diatoms.

Author contributions

JJM, SA and SPA designed the experiments. L. Pichevin cleaned the diatoms. SPA prepared the samples and conducted NanoSIMS analyses. GD performed the Raman analyses. SPA and L. Polerecky performed NanoSIMS data analysis. GD and SPA performed the Raman data analyses. SPA interpreted the data, prepared the figures and wrote the manuscript text with contributions from all authors.

Declaration of Competing Interest

The authors declare that they have no known competing financial interests or personal relationships that could have appeared to influence the work reported in this paper.

Acknowledgments

We would like to thank M. Kienhuis for analytical support. The NanoSIMS facility at Utrecht University was financed through a large infrastructure grant by the Netherlands Organisation for Scientific Research (NWO) (grant no. 175.010.2009.011). This work was carried out under the programme of the Netherlands Earth System Science Centre (NESSC), financially supported by the Ministry of Education, Culture and Science (OCW) in the Netherlands (grant no. 024.002.001). This study was further supported by the King Abdullah University of Science and Technology baseline funding to SA (BAS/1/1072-01-01).

Appendix A. Supplementary data

Supplementary data to this article can be found online at https://doi.org/10.1016/j.marchem.2020.103906.

References

Bridoux, M.C., Ingalls, A.E., 2010. Structural identification of long-chain polyamines associated with diatom biosilica in a Southern Ocean sediment core. Geochim. Cosmochim. Acta 74, 4044–4057. https://doi.org/10.1016/j.gca.2010.04.010.

De La Rocha, C.L., 2006. Opal-based isotopic proxies of paleoenvironmental conditions. Glob. Biogeochem. Cycles 20, 1–11. https://doi.org/10.1029/2005GB002664.

De Tommasi, E., Congestri, R., Dardano, P., De Luca, A.C., Managò, S., Rea, I., De Stefano, M., 2018. UV-shielding and wavelength conversion by centric diatom nanopatterned frustules. Sci. Rep. 8, 16285. https://doi.org/10.1038/s41598-018-34651-w.

Des Combes, H.J., Esper, O., De La Rocha, C.L., Abelmann, A., Gersonde, R., Yam, R., Shemesh, A., 2008. Diatom δ13C, δ15N, and C/N since the last glacial maximum in the southern ocean: potential impact of species composition. Paleoceanography 23, 1–12. https://doi.org/10.1029/2008PA001589.

Ellwood, M.J., Hunter, K.A., 1999. Determination of the Zn/Si ratio in diatom opal: a method for the separation, cleaning and dissolution of diatoms. Mar. Chem. 66, 149–160.

Hecky, R.E., Mopper, K., Kilham, P., Degens, E.T., 1973. The amino acid and sugar composition of diatom cell walls. Mar. Biol. 19, 323.

Hendry, K.R., Rickaby, R.E.M., 2008. Opal (Zn/Si) ratios as a nearshore geochemical proxy in coastal Antarctica. Paleoceanography 23, 1–12. https://doi.org/10.1029/2007PA001576.

Hildebrand, M., Lerch, S.J.L., Shrestha, R.P., 2018. Understanding diatom cell wall silicification-moving forward. Front. Mar. Sci. https://doi.org/10.3389/fmars.2018.00125.

Horn, M.G., Beucher, C.P., Robinson, R.S., Brzezinski, M.A., 2011a. Southern Ocean nitrogen and silicon dynamics during the last deglaciation. Earth Planet. Sci. Lett. 310, 334–339. https://doi.org/10.1016/j.epsl.2011.08.016.

Horn, M.G., Robinson, R.S., Rynearson, T.A., Sigman, D.M., 2011b. Nitrogen isotopic relationship between diatom-bound and bulk organic matter of cultured polar diatoms. Paleoceanography 26, 1–12. https://doi.org/10.1029/2010PA002080.

Ingalls, A.E., Lee, C., Wakeham, S.G., Hedges, J.I., 2003. The role of biominerals in the sinking flux and preservation of amino acids in the Southern Ocean along 170°W. Deep. Res. Part II Top. Stud. Oceanogr. 50, 713–738. https://doi.org/10.1016/S0967-0645(02)00592-1.

Kammer, M., Hedrich, R., Ehrlich, H., Popp, J., Brunner, E., Krafft, C., 2010. Spatially resolved determination of the structure and composition of diatom cell walls by Raman and FTIR imaging. Anal. Bioanal. Chem. 398, 509–517. https://doi.org/10.1007/s00216-010-3924-0.

Kröger, N., Poulsen, N., 2008. Diatoms—from cell wall biogenesis to nanotechnology. Annu. Rev. Genet. 42, 83–107. https://doi.org/10.1146/annurev.genet.41.110306.130109.

Kröger, N., Lorenz, S., Brunner, E., Sumper, M., 2002. Self-assembly of highly phosphorylated silaffins and their function in biosilica morphogenesis. Science 298, 584–586.

Liang, Z., Yin, Z., Yang, H., Xiao, Y., Hang, W., Li, J., 2016. Nanoscale surface analysis that combines scanning probe microscopy and mass spectrometry: a critical review. Trends Anal. Chem. https://doi.org/10.1016/j.trac.2015.07.009.

Lin-Vien, D., Colthup, N.B., Fateley, W.G., Grasselli, J.G., 1991. Double bonds containing nitrogen atoms in: the handbook of infrared and Raman characteristic frequencies of organic molecules. Elsevier, pp. 191–212.

McMillan, P., Piriou, B., Navrotsky, A., 1982. A Raman spectroscopic study of glasses along the joins silica-calcium aluminate, silica-sodium aluminate, and silica-potassium aluminate. Geochim. Cosmochim. Acta 46, 2021–2037. https://doi.org/10.1016/0016-7037(82)90182-X.

Morley, D.W., Leng, M.J., Mackay, A.W., Sloane, H.J., Rioual, P., Battarbee, R.W., 2004. Cleaning of lake sediment samples for diatom oxygen isotope analysis. J. Paleolimnol. 31, 391–401. https://doi.org/10.1023/B:JOPL.0000021854.70714.6b.

Nuñez, J., Renslow, R., Cliff, J.B., Anderton, C.R., 2018. NanoSIMS for biological applications: current practices and analyses. Biointerphases 13, 03B301. https://doi.org/10.1116/1.4993628.

Pichevin, L., Ganeshram, R.S., Reynolds, B.C., Prahl, F., Pedersen, T.F., Thunell, R., McClymont, E.L., 2012. Silicic acid biogeochemistry in the Gulf of California: insights from sedimentary Si isotopes. Paleoceanography 27, 1–14. https://doi.org/10.1029/2011PA002237.

Pichevin, L.E., Ganeshram, R.S., Geibert, W., Thunell, R., Hinton, R., 2014. Silica burial enhanced by iron limitation in oceanic upwelling margins. Nat. Geosci. 7, 8–13. https://doi.org/10.1038/ngeo2181.

Polerecky, L., Adam, B., Milucka, J., Musat, N., Vagner, T., Kuypers, M.M.M., 2012. Look@NanoSIMS - a tool for the analysis of nanoSIMS data in environmental microbiology. Environ. Microbiol. 14, 1009–1023. https://doi.org/10.1111/j.1462-2920.2011.02681.x.

Ren, H., Brunelle, B.G., Sigman, D.M., Robinson, R.S., 2013. Diagenetic aluminum uptake into diatom frustules and the preservation of diatom-bound organic nitrogen. Mar. Chem. 155, 92–101. https://doi.org/10.1016/j.marchem.2013.05.016.

Robinson, R.S., Brunelle, B.G., Sigman, D.M., 2004. Revisiting nutrient utilization in the glacial Antarctic: evidence from a new method for diatom-bound N isotopic analysis. Paleoceanography 19, 1–13. https://doi.org/10.1029/2003PA000996.

Robinson, R.S., Brzezinski, M.A., Beucher, C.P., Horn, M.G.S., Bedsole, P., 2014. The changing roles of iron and vertical mixing in regulating nitrogen and silicon cycling in the Southern Ocean over the last glacial cycle. Paleoceanography 29, 1179–1195. https://doi.org/10.1002/2014PA002686.

Roepert, A., 2019. Imaging element distributions within small marine calcifiers: a NanoSIMS perspective. Utrecht Studies Earth Sci. 201 (ISBN 978-90-6266-560-0).

Shemesh, A., Macko, S.A., Charles, C.D., Rau, G.H., 1993. Isotopic evidence for reduced productivity in the glacial Southern Ocean. Science 262, 407–410. https://doi.org/10.1126/science.262.5132.407.

Sigman, D.M., Altabet, M.A., Francois, R., McCorkle, D.C., Gaillard, J.F., 1999. The isotopic composition of diatom-bound nitrogen in Southern Ocean sediments. Paleoceanography 14, 118–134. https://doi.org/10.1029/1998PA900018.

Terpstra, P., Combes, D., Zwick, A., 1990. Effect of salts on dynamics of water: A Raman spectroscopy study. J. Chem. Phys. 92, 65–70. https://doi.org/10.1063/1.458418.

Tesson, B., Hildebrand, M., 2013. Characterization and localization of insoluble organic matrices associated with diatom cell walls: insight into their roles during cell wall formation. PLoS One 8. https://doi.org/10.1371/journal.pone.0061675.

Thamatrakoln, K., Hildebrand, M., 2008. Silicon uptake in diatoms revisited: a model for saturable and nonsaturable uptake kinetics and the role of silicon transporters. Plant Physiol. 146, 1397–1407. https://doi.org/10.1104/pp.107.107094.